Theoretical analysis of the characteristics of critical heat flux in vertical narrow rectangular channels under motion conditions

Mengmeng Xi[1], Wenxi Tian[1], Siyang Huang[1], Guanghui Su[1], Suizheng Qiu[1], Dongxiao Du[2]

[1]: Department of Nuclear Science and Technology, Xi'an Jiaotong University, 710049
No.28 Xianning west road, Xi'an, China

[2]: Shanghai Nuclear Engineering Research and Design Institute, 200233
Shanghai, China

Email: ximengmeng1990@stu.xjtu.edu.cn

Abstract

A mathematical three-fluid model of annular upward flow including additional forces of ocean conditions has been developed to predict the critical heat flux (CHF) in uniformly heated vertical narrow rectangular channels. The mathematical model is based on fundamental conservation principles: the mass and momentum conservation equation of the liquid film, liquid droplets and the vapor core and the mass and momentum transfers between the three-fluid together with a set of closure relationships. An analysis code with Visual Fortran 6.5 has been developed. The effects of motion and inlet mass flux fluctuation on the CHF are analyzed, respectively. Comparisons between prediction results and experimental data show good precision and accuracy. With the applications of the present code, the influences of the amplitude and period of inlet mass flux fluctuation on the CHF in rectangular channels are analyzed, respectively. The influences of the amplitude and period of heaving and rolling motion on the CHF are also investigated. The obtained analysis results are significant to the improvement of design and safety operation of the reactor system.

Keywords: Effect of additional acceleration, Critical heat flux, Vertical narrow rectangular channel, uniformly heated

Nomenclature

A	cross-sectional area of channel, m^2	h_{fg}	latent heat of vaporization, kJ/kg
De	hydraulic diameter of channel, m	P_{rq}	heating periphery, m
D_{ep}	liquid droplets deposition rate, kg/(m^2s)	P_{rw}	channel periphery, m
E_{nh}	liquid droplets wave entrainment rate, kg/(m^2s)	M_{wf}	wall friction
E_{nq}	liquid droplets boiling entrainment rate, kg/(m^2s)	M_{fg}	vapor-liquid interface friction
Re	Reynolds number dimensionless	M_{gd}	friction between the vapor core and droplets
g	gravitational acceleration, m/s^2	*Greek symbols*	
G	mass flux, kg/(m^2s)	α	void fraction dimensionless
p	pressure, MPa	ρ	density, kg/m^3
$\boldsymbol{F}$	additional forces of ocean motions, N/m^3	θ	rolling angle, rad
$\boldsymbol{f}$	body force, N/m^3	ω	angular velocity, rad/s
t	time, s	β	angular acceleration, rad/s^2
u	velocity, m/s	*Subscripts*	

q_{CHF}	critical heat flux, kW/m^2	f	liquid film
L	heating length, m	d	droplets
		g	vapor core

1. Introduction

Critical heat flux (CHF) is an important design factor in designing marine-mounted nuclear reactor system to ensure the safety operation. In the vertical upward channel, there are several changes from inlet to exit in the flow pattern of coolant. The liquid film thickness of annular flow will decrease with the comprehensive effects of vaporization of the liquid film, deposition and entrainment of droplets. When the liquid film thickness decreases to a certain value (10^{-9}), the surface temperature will rise suddenly due to the decrease of heat transfer coefficient, and then boiling crisis will occur. Boiling crisis occurring in an annular flow is called dryout, and the heat flux just before dryout is called CHF. The main difference between a land-based and marine-mounted reactor system is the influence of sea wave oscillations on the latter. Oscillations change the effective forces acting on the fluid and induce flow fluctuations, which result in a change in momentum, heat and mass transfer characteristics (Pendyala et al 2008). The CHF under motion conditions is different from that under static condition. Because of the complexity of ocean motions, the theoretical research is not enough. Research in the characteristics of CHF under ocean motions is of significant interest to the design, safety analysis and improvement of overall performance of the marine-mounted nuclear reactor system.

Presently, there are limited experimental research for the CHF under motion condition. Researchers usually adopt the method of empirical correlation to modify the CHF value of the nuclear system because of the complexity of ocean motions.

Otsuji T et al. studied the influence of periodically varying acceleration on CHF of Freon-113 flowing upward in a uniformly heated vertical annular channel experimentally (Otsuji & Kurosawa 1982). In their experiment, the Freon loop was oscillated vertically to determine the ratio of CHF in the oscillating acceleration field to the corresponding stationary value. The amplitude of inlet mass flux fluctuation induced by variation of acceleration will cause a reduction in the CHF, and the reduction is proportional to the acceleration amplitude. The CHF is effected by inlet subcooling and exit quality. Nevertheless the degradation of CHF is more remarkable in the low quality region. Pang Fengge et al. conducted forced circulation experiments at atmospheric pressure to study the influence of swing on the CHF (Pang Fengge, et al 1997). The results of their study indicated that the CHF under swing condition occurred earlier than that under static condition, and the CHF under swing condition could be remarkably lower than that under static condition in forced circulation. Wang Jie reported their CHF experiment of water in a single heated tube at heaving and swing conditions at medium pressure (Wang Jie, 2001). During his experiment, we could observe that ocean conditions have obvious influence on the CHF at medium pressure. The experimental results show that rolling motion can cause the burnout to occur earlier than that without rolling motion and cause a decrease in the CHF. The effect of rolling upon CHF is different with different mass velocities. It can be assumed that the ocean conditions have obvious influence on CHF at medium pressure.

Some theoretical analysis has been done to study the influence of ocean conditions on the CHF. The effect of different ocean motions on coolant flow can come down to different additional forces in the momentum equation, thus ocean conditions can be considered by adding additional forces to the momentum equation. Qian Libo et al. developed the model of additional forces of 6 types of typical and relevant coupled ocean conditions based on the basic momentum

equation in the non-inertial reference frame and the one-dimensional coolant channel (Qian Libo et al, 2012). Liu WX et al. investigated the influence of the new arisen acceleration field created by ocean conditions on the occurrence of critical heat flux (CHF), and proposed an improved model based on microscopic mechanism of bubble dynamics developed with the liquid sublayer dryout mechanism (Liu et al, 2012). Vladimir Stevanovic used three-fluid model to simulate the vertical annular two phase flow (Vladimir Stevanovic et al, 1994). The three-fluid model was presented for the prediction of dryout and post-dryout heat transfer at high pressure conditions (Sreenivas Jayanti et al, 2003). A FIDAS code with three-fluid model has been developed to predict dryout and post-dryout heat transfer in a channel and in rod bundles (Satoru Sugawara et al, 1990).

Literature reviews indicate that only a little research has been carried out under motion conditions. It is necessary to study the CHF under motion condition. We define the minimum heat flux which makes the the minimum value of liquid film flow at the outlet equal to zero as CHF. Thus, by taking account of the influence of ocean motions, a mathematical model has been developed and numerically calculated. The influences of ocean conditions on the CHF are analyzed.

2. Mathematical model

2.1 The momentum conservation equation under motion conditions

The momentum conservation equation under motion conditions can be written as

$$\frac{D(\rho u)}{Dt} = -\frac{\partial p}{\partial z} - \frac{f}{D_e}\frac{\rho u^2}{2} + (\boldsymbol{F} + \rho \boldsymbol{f})\cdot \boldsymbol{k} \tag{1}$$

where $\boldsymbol{F}$ is additional forces of ocean motions.

Heaving motion is that the ship moves in the z axis vertical direction with a certain acceleration $a_{0,}$ as shown in Fig.1. The acceleration is $a_0=a_z(t)\boldsymbol{k}$.

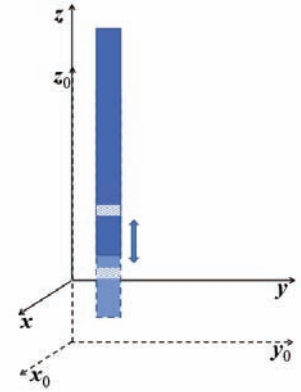

Fig. 1 Schematic of the heaving motion

The influence of the heaving motion can be written as:

$$(\boldsymbol{F}+\rho \boldsymbol{f})\cdot \boldsymbol{k} = (-\rho a_z(t)\boldsymbol{k} - \rho g \boldsymbol{k})\cdot \boldsymbol{k} = -\rho(a_z(t)+g) \tag{2}$$

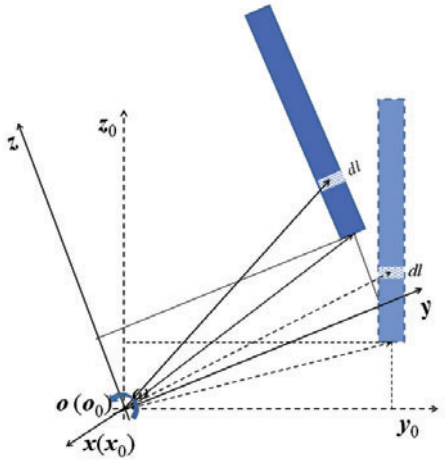

Fig. 2 Schematic of the rolling motion

Rolling motion is that the ship rotates at a certain angular velocity around the *x* axis in the *yz* plane. As shown in Fig. 2, the angle velocity and acceleration is $\boldsymbol{\omega}=\omega_x(t)\boldsymbol{i}$ and $\boldsymbol{\beta}=\beta_x(t)\boldsymbol{i}$.

The influence of rolling motion can be written as

$$(\boldsymbol{F}+\rho\boldsymbol{f})\cdot\boldsymbol{k}=-\rho\left(g\cos\theta(t)+\beta_x(t)y-\omega_x^{\ 2}(t)z\right) \tag{3}$$

where $\theta(t)$ is the rolling angle.

The additional force caused by rolling motion is not related to rolling angle velocity and acceleration, but also the location of the fluid particle.

2.2 The three-fluid model

In an annular flow regime of narrow rectangular channels, the liquid flows upward adhered to the channel walls forming a continuous annular liquid film. The vapor with entrained droplets flows along the center of the channel, and forms a continuous vapor core. Mass is continuously exchanged between the liquid film and droplets entrained in the vapor core in the flow direction: droplets entrained in the vapor core deposit to the liquid film, and the vapor core of high velocity flow cause droplets entrainment in the liquid film.

2.2.1 Mass conservation equations

(1)The mass conservation equation of the liquid film

In the annular region, there exists mass transfer at the liquid film-vapor core interface by the complicated effects on film evaporation, droplets entrainment and deposition. The mass conservation equation of the liquid film is shown as follow

$$\frac{\partial}{\partial\tau}\left(\rho_f\alpha_f\right)+\frac{\partial\left(\rho_f\alpha_f u_f\right)}{\partial z}=-\frac{qP_{rq}}{Ah_{fg}}+\frac{P_{rw}D_{\mathrm{ep}}-(P_{\mathrm{rw}}E_{\mathrm{nh}}+P_{\mathrm{rq}}E_{\mathrm{nq}})}{A} \tag{4}$$

where ρ_f is the density of the liquid film, α_f the void fraction of the liquid film, u_f is the average flow velocity of the liquid film, q is the heat flux, h_{fg} is the latent heat of vaporization, A is the cross-sectional area of rectangular channel, P_{rw} is the channel periphery, P_{rq} is the heating periphery, D_{ep} is the liquid droplets deposition rate per unit area, E_{nh} is the liquid droplets

entrainment rate per unit area caused by breakup of disturbance waves on the liquid film-vapor core interface, E_{nq} is the liquid droplets entrainment rate per unit area induced by burst of boiling bubbles in the liquid film.

(2)The mass conservation equation of droplets

Droplets come from the liquid film evaporation, droplets entrainment and deposition,

$$\frac{\partial}{\partial \tau}\left(\rho_d \alpha_d\right)+\frac{\partial\left(\rho_d \alpha_d u_d\right)}{\partial z}=-\frac{P_{rw} D_{\mathrm{ep}}-\left(P_{\mathrm{rw}} E_{\mathrm{nh}}+P_{\mathrm{rq}} E_{\mathrm{nq}}\right)}{A} \tag{5}$$

where ρ_d is the density of droplets, α_d is the void fraction of droplets, and u_d is the average flow velocity of droplets.

(3)The mass conservation equation of the vapor core

The vapor core of the annular flow region mainly comes from the liquid film evaporation,

$$\frac{\partial}{\partial \tau}\left(\rho_g \alpha_g\right)+\frac{\partial\left(\rho_g \alpha_g u_g\right)}{\partial z}=\frac{q P_{rq}}{A h_{fg}} \tag{6}$$

where ρ_g is the density of the vapor core, α_g is the void fraction of the vapor core, and u_g is the average flow velocity of the vapor core.

2.2.2 Momentum conservation equations

(1)The momentum conservation equation of the liquid film

According to the law of momentum conservation on the liquid film control volume in which frictional force between the liquid film and droplets is ignored, the momentum conservation equation is deduced as follow:

$$\begin{aligned}&\frac{\partial(\rho_f \alpha_f u_f)}{\partial \tau}+\frac{\partial(\rho_f \alpha_f u_f^2)}{\partial z}-\frac{D_{ep} P_{rw}}{A} u_d+\frac{q P_{rq}}{A h_{fg}} u_f+\frac{E_{nh} P_{rw}+E_{nq} P_{rq}}{A} u_f \\ &=-\alpha_f \frac{\partial p}{\partial z}+\alpha_f(\boldsymbol{F}+\rho_f \boldsymbol{f}) \cdot \boldsymbol{k}-M_{wf}+M_{fg}\end{aligned} \tag{7}$$

Where M_{wf} is the wall friction, M_{fg} is the vapor-liquid interface friction.

(2)The momentum conservation equation of droplets

The forces of droplets include: gravity, pressure and frictional force between the vapor core and droplets. According to the forces of droplets and momentum exchange between droplets and the liquid film, the momentum conservation equation of droplets is deduced as follow:

$$\begin{aligned}&\frac{\partial(\rho_d \alpha_d u_d)}{\partial \tau}+\frac{\partial(\rho_d \alpha_d u_d^2)}{\partial z}+\frac{D_{ep} P_{rw}}{A} u_d-\frac{E_{nh} P_{rw}+E_{nq} P_{rq}}{A} u_f \\ &=-\alpha_d \frac{\partial p}{\partial z}+\alpha_d(\boldsymbol{F}+\rho_d \boldsymbol{f}) \cdot \boldsymbol{k}+M_{gd}\end{aligned} \tag{8}$$

where M_{gd} is the friction between the vapor core and droplets.

(3)The momentum conservation equation of the vapor core

The forces of the vapor core include: gravity, pressure, frictional force between the vapor core and droplets and frictional force between the vapor core and the liquid film. According to the force of the vapor core and momentum exchange between the vapor core and the liquid film, the momentum conservation equation of the vapor core is deduced as follows:

$$\frac{\partial(\rho_g \alpha_g u_g)}{\partial \tau} + \frac{\partial(\rho_g \alpha_g u_g^2)}{\partial z} - \frac{qP_{rq}}{Ah_{fg}} u_f = -\alpha_g \frac{\partial p}{\partial z} + \alpha_g (\boldsymbol{F} + \rho_g \boldsymbol{f}) \cdot \boldsymbol{k} - M_{fg} - M_{gd} \quad (9)$$

In order to simplify the three-fluid model, it is assumed that the liquid film, droplets and the vapor core of annular upward flow are in saturated condition.

2.2.3 The void fraction

The relation of the void fractions of the liquid film, droplets and the vapor core in annular flow is given as:

$$\alpha_f + \alpha_d + \alpha_g = 1 \quad (10)$$

2.2.4 Equations of the interfacial friction

The interfacial friction between the liquid film and the wall can be expressed as follow;

$$M_{wf} = \frac{1}{A} \frac{f_w \rho_f |u_f| u_f}{2} P_r \quad (11)$$

where the friction coefficient can be calculated by Wallis correlation (Wallis GB, 1969).

$$f_w = \max(\frac{16}{Re_f}, 0.005)$$

$$Re_f = \alpha_f \rho_f u_f De / \mu_f$$

where De is the hydraulic equivalent diameter of the rectangle channel, and μ_f is dynamic viscosity of the liquid film.

The interfacial friction between the liquid film and the vapour core can be calculated by:

$$M_{fg} = \frac{1}{2A} f_{fg} \rho_g |u_g - u_f| (u_g - u_f) P_{r,fg} \quad (12)$$

where the friction coefficient can be calculated by Wallis correlation (Wallis GB, 1969)

$$f_{fg} = 0.005(1 + 300 \frac{\delta}{De})$$

The interfacial friction between droplets and the vapour core

$$M_{gd} = \frac{1}{8} C_d a_{gd} \rho_g |u_g - u_d| (u_g - u_d) \quad (13)$$

where C_d is droplets drag coefficient, a_{gd} is interfacial coefficient.

a_{gd} can be calculated as follow:

$$a_{gd} = 6\alpha_d / De_d$$

C_d is expressed by Clift coefficient (Clift R et al. 1978)

$$C_d = \frac{24}{Re_d}(1 + 0.15 Re_d^{0.687}) + \frac{0.42}{1 + 4.25 \times 10^4 Re_d^{-1.16}}$$

where $Re_d = \rho_g |u_g - u_d| De_d / \mu_g$, D_{ed}=0.1mm

2.2.5 Entrainment and deposition model

The entrainment and deposition in the model are calculated by Okawa correlations (Okawa T, 2004).

Okawa & Kotani think the deposition rate is proportional to the droplet concentration in the gas core C

$$D_{\mathrm{ep}} = k_d C \tag{14}$$

It is considered that the formation of droplets entrainment is caused by two different mechanisms: the wave entrainment (E_{nh}) caused by breakup of disturbance waves on the liquid film-vapor core interface due to interfacial shear force; and the boiling entrainment (E_{nq}) induced by burst of boiling bubbles in the liquid film. The wave entrainment rate E_{nh} is evaluated with the following equations:

$$E_{\mathrm{nh}} = k_e \rho_f \pi_e^n \tag{15}$$

The correlation of Milashenko et al. was adopted in the present model due to its wider applicability:

$$E_{\mathrm{nq}} = \frac{1.75 W_f}{(\pi De)^2}\left[q \times 10^{-3}\left(\frac{\rho_g}{\rho_f} \right) \right]^{1.3} \tag{16}$$

3. Results and discussion

3.1 Validation and verification of the model under steady state

To identify the range of validity and accuracy of the model proposed in this paper, the CHF prediction correlation in circular tube proposed by Katto and the experiment data of CHF value in rectangle channel are employed. The correlation proposed by Katto is described as follow:

$$q_{CHF} = 0.234 G h_{fg}\left(\frac{\rho_g}{\rho_f} \right)^{0.513}\left(\frac{\sigma \rho_f}{G^2 L} \right)^{0.433} \frac{\left(L/De \right)^{0.27}}{1 + 0.0031 L/De} \tag{17}$$

The CHF values predicted by our model and the correlation are compared in different equivalent diameters, channel lengths, system pressures and mass flux. The detailed comparison between predicted results and correlation data is shown in Fig. 3. It can be seen that the predicted values show good agreement with the Katto correlation. Meanwhile, the predicted CHF values and experimental data in rectangular channel are compared in Fig. 4. As shown in Fig. 4, the forecasting error is within 20%. The results present that the model can well predict CHF characteristics in rectangular channel.

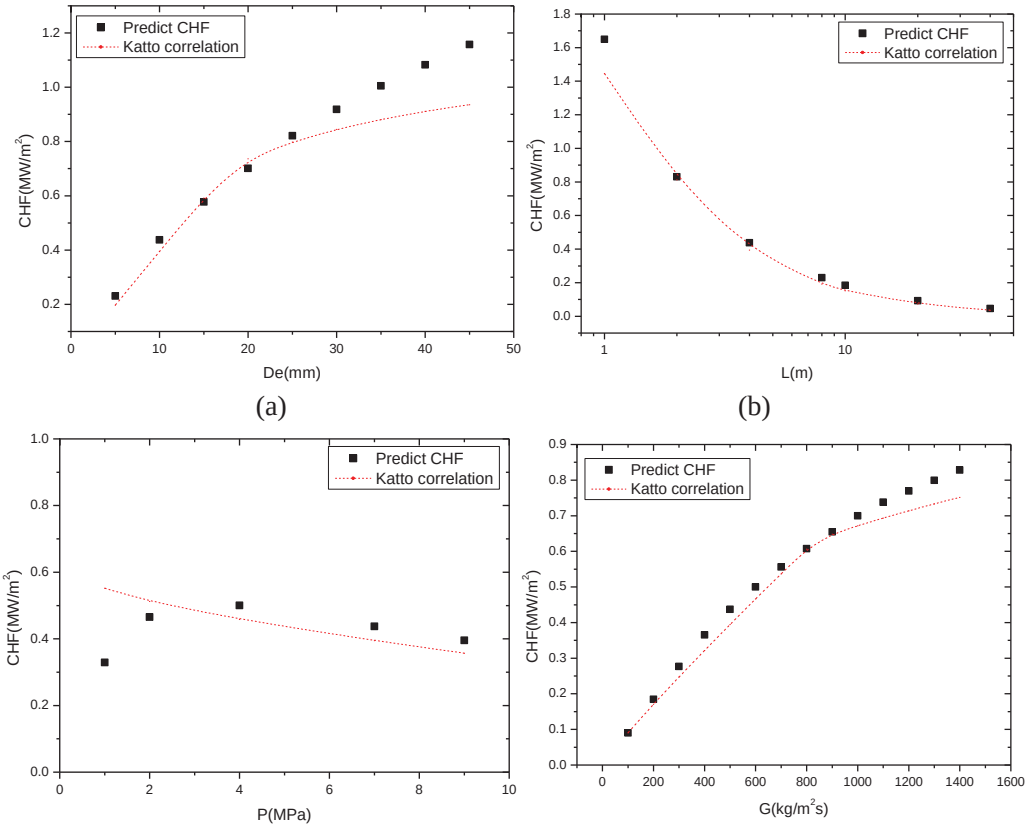

Fig. 3 Comparisions between predictd CHF values and Katto correlation in circular tube. (a) Respect to equivalent diameter; (b) Respect to channel length; (c) Respect to system pressure; (d) Respect to mass flux.

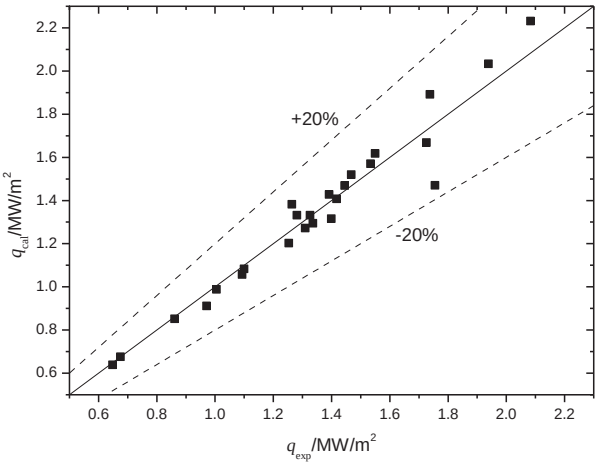

Fig. 4 Comparisions between predictd CHF values and experimental data in rectangular channel

3.2 The characteristics of CHF under flow fluctuation condition

The system mass flux of the forced circulation system under heaving and rolling motions have been studied experimentally by many researchers. Their research results show that the period of the system mass flux fluctuation as expected equals to that of the heaving and rolling

motion. The characteristics of CHF under flow fluctuation condition are studied in this section. The inlet mass flux can be expressed as follow：

$$G_{in} = G_{\mathrm{AVE}} + \Delta G \sin(\frac{2\pi}{T_{OSC}} t) \tag{18}$$

where G_{in} is the inlet mass flux, G_{AVE} is the average mass flux, ΔG is the amplitude of mass flux fluctuation, T_{OSC} is the period of mass flux fluctuation, and t is time.

The variations of the total mass flux, the mass flux of the liquid film, droplets and the vapor core along the flow direction in rectangular channel are shown in Fig. 5. Different curves in Fig. 5 represent mass flux at different times in one period. It can be seen from the Fig. 5(a) that the inlet mass flux fluctuate in the range of $\pm \Delta G$ in the average value of G_{AVE}. The fluctuation amplitude of the total mass flux decreases in the flow direction because of axial roll of the liquid film and droplets entrainment. The fluctuation amplitude of the total mass flux at the outlet is obviously lower than that at the inlet. As shown in Fig. 5(b-d), the mass flux of the liquid film decrease in the flow direction, the mass flux of droplets increase in the flow direction, and the mass flux of the vapor core increase linearly in the flow direction. It can be seen that the influence of the inlet mass flux fluctuation on the variation of mass flux of the vapor core is much less.

Fig. 6 presents the relation between the total mass flux at the outlet and time. The fluctuation amplitude of the mass flux at the outlet is obviously less than that at the inlet, as shown in Fig. 6. It can also be noted that the fluctuation period of the mass flux at the outlet is the same with that at the inlet, but there is a phase difference between them. These results are consistent with the Fig. 5(a).

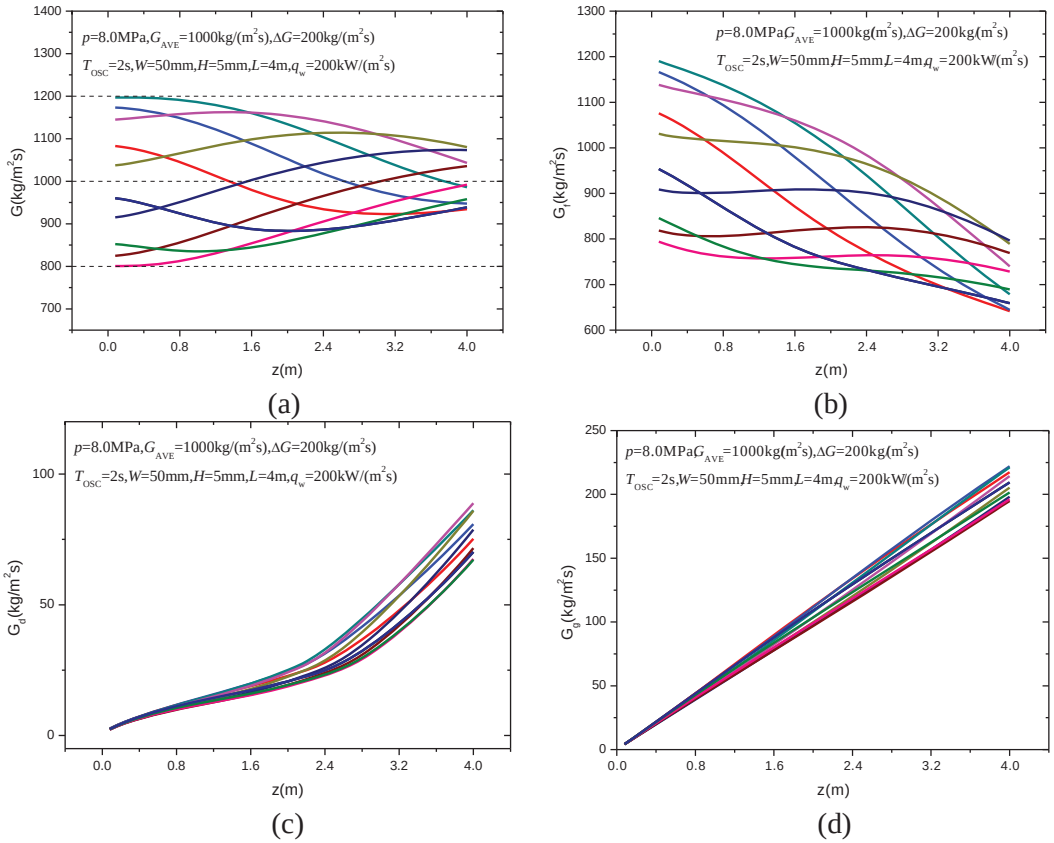

Fig. 5 Relations between mass flux and the flow direction at different moment. (a) Relation between the total mass flux and the flow direction. (b) Relation between the mass flux of the liquid film and the flow direction. (c) Relation between the mass flux of droplets and the flow direction. (d) Relation between the mass flux of the vapor core and the flow direction.

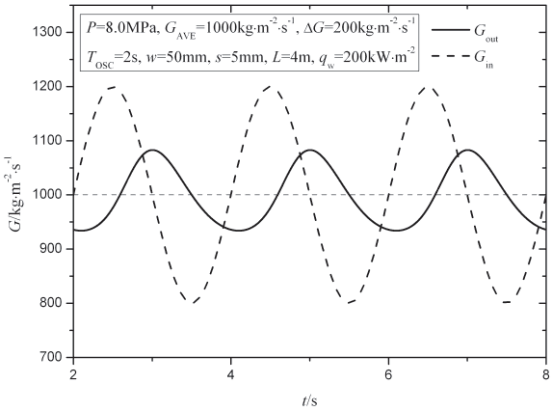

Fig. 6 Relation between the total mass flux at outlet and time

The characteristic of CHF under flow fluctuation condition is shown in Fig. 7. It can be observed that the CHF decreases with an increase in the flow fluctuation amplitude, and the CHF under low flow fluctuation amplitude is close to the CHF when the inlet mass flux is G_{AVE}- Δ G.

Fig. 8 shows the relation between CHF and the fluctuation period. As shown in Fig. 8, the CHF decreases with an increase in the fluctuation period, and the CHF value under high fluctuation period is close to the CHF value when the inlet mass flux is G_{AVE}- Δ G.

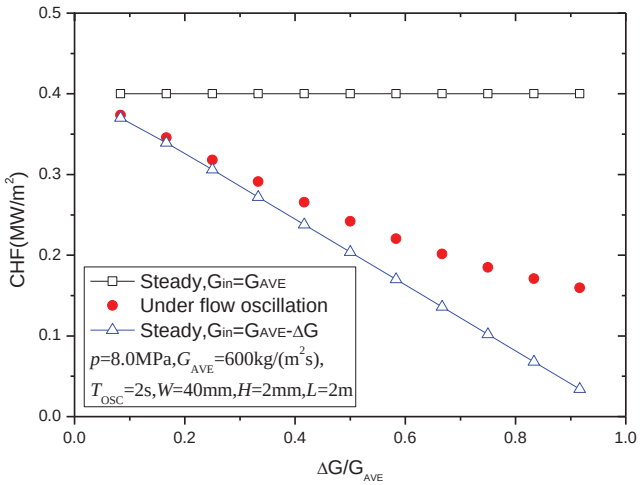

Fig. 7 Relation between CHF and the fluctuation amplitude

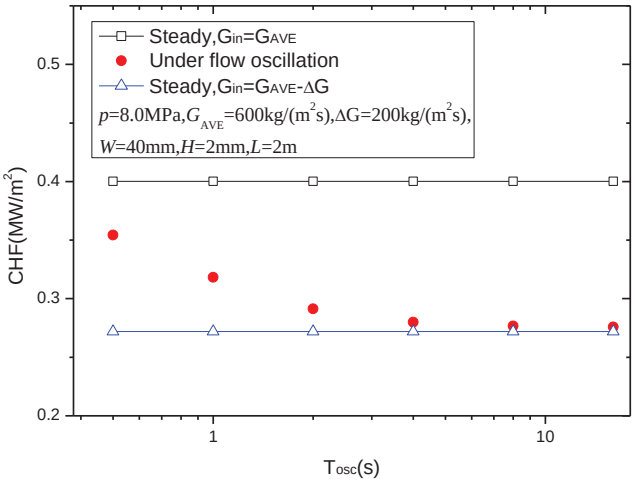

Fig. 8 Relation between CHF and the fluctuation period

3.3 Influence of ocean motion on the characteristics of CHF

In this section, the influence of different ocean motions on the characteristics of CHF without considering the inlet flow fluctuation is investigated.

Fig. 9 shows the relation between the mass flux of the liquid film at the outlet and time for different heaving amplitudes and periods. It can be observed that the mass flux of the liquid film at the outlet fluctuates with time in cycles. The fluctuation amplitude increases with an increase in the heaving amplitude, decreases with an increase in the heaving period, as clearly shown in Fig. 9. This is because the additional force caused by the heaving motion leads to a pressure variation in the channel, which affects deposition rate and entrainment rate of droplets and evaporation of the liquid film.

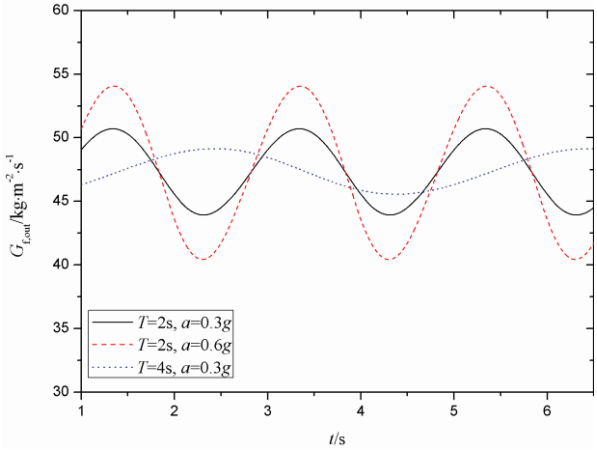

Fig. 9 Influence of the heaving amplitude and period on the mass flux of the liquid film at the outlet

The characteristics of CHF under heaving motion is shown in Fig. 10. It can been seen that the CHF decreases with an increase in the heaving amplitude, increases with an increase in the heaving period under the same heaving amplitude, which indicates that the influence of the heaving motion is less with the increasing of the heaving period.

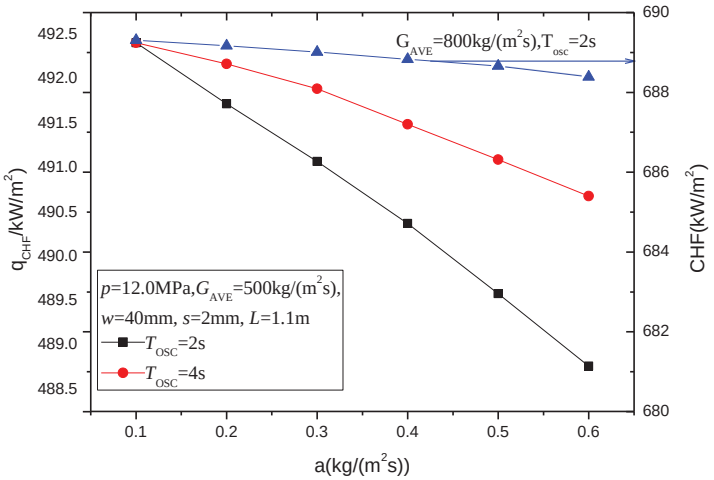

Fig. 10 the characteristics of CHF under heaving motion

The angular displacement, angular velocity and angular acceleration under the rolling motion can be expressed as follows:

$$\theta(t) = \theta_m \sin(\frac{2\pi}{T}t) \tag{19}$$

$$\omega(t) = \frac{\partial\theta}{\partial t} = \theta_m \frac{2\pi}{T}\cos(\frac{2\pi}{T}t) \tag{20}$$

$$\beta(t) = \frac{\partial^2\theta}{\partial t^2} = -\theta_m\left(\frac{2\pi}{T}\right)^2 \sin(\frac{2\pi}{T}t) \tag{21}$$

where θ_m is the rolling amplitude, T is the rolling period, and t is time.

Fig. 11 presents the simulation of the influence of the rolling amplitude and period on the mass flux of the liquid film at the outlet. From the Fig. 11, the fluctuation amplitude of the mass flux increases as the rolling amplitude increases, decreases as the rolling period increases.

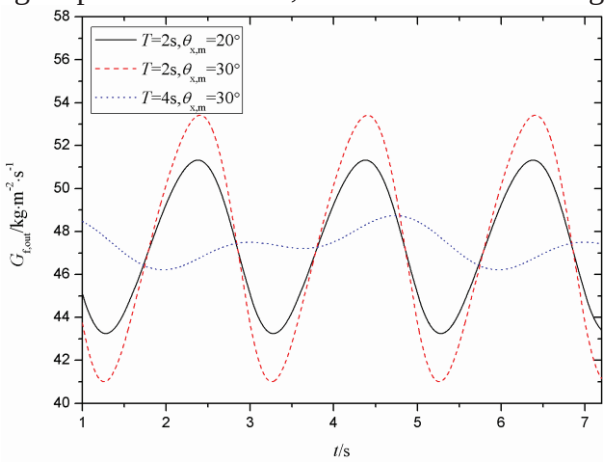

Fig. 11 Influence of the rolling amplitude and period on the mass flux of the liquid film at the outlet

The influence of rolling motion on CHF is shown in Fig. 12. The CHF value decreases with an increase in rolling motion amplitude, as shown in Fig. 12. It can also be observed that the CHF value increases with an increase in rolling motion period under the same rolling motion amplitude.

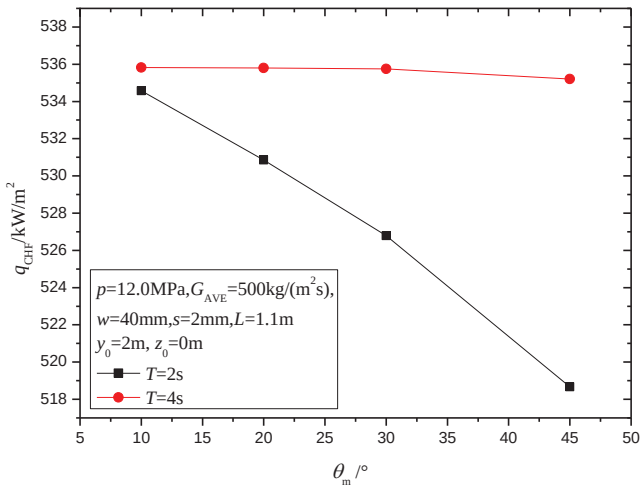

Fig. 12 the characteristics of CHF under rolling motion

4. Conclusion

A mathematical three-fluid model of annular upward flow has been developed to investigate the characteristics of the CHF under ocean motion condition. By numerically solving the proposed model, the CHF can be predicted well comparing with experimental data under steady state. The influence of inlet flow fluctuation and ocean motions on the characteristics of CHF are studied, respectively. Several important conclusions can be drawn through analyzing the results:

(1) The CHF decreases as the fluctuation amplitude and period increase under flow fluctuation condition.

(2) The CHF decreases with an increase in the heaving amplitude, while increases with an increase in the heaving period under the same heaving amplitude.

(3) The CHF decreases with an increase in the rolling amplitude, while increases with an increase in the rolling period under the same rolling amplitude.

References

[1]Pendyala R, Jayanti S, Balakrishnan AR. 2008. Flow and pressure drop fluctuations in a vertical tube subject to low frequency oscillations. Nuclear Engineering and Design 238:178-87.
[2]Otsuji T, Kurosawa A. 1982. Critical heat flux of forced convection boiling in an oscillating acceleration field — I. General trends. Nuclear Engineering and Design 71:15-26.
[3]Pang Fengge, Gao Puzhen, Wang Zhaoxiang, et al. 1997. Experimental investigation on effect of rolling upon critical heat flux (CHF) for water at atmospheric pressure. Chinese Journal of Nuclear Science and Engineering: 367-71. (In Chinese).
[4]Wang Jie. 2001. Experimental investigation on effect of rolling upon critical heat flux (CHF) in single channel [M]. Harbin Engineering University.
[5]Qian Libo, Tian Wenxi Qiu Suizheng, et al. 2012. Research on model of additional forces of ocean conditions in one-dimensional coolant channel. Nuclear Power Engineering 33:104-9. (In Chinese)
[6]Liu WX, Tian WX, Wu YW, Su GH, Qiu SZ, et al. 2012. An improved mechanistic critical heat flux model and its application to motion conditions. Progress in Nuclear Energy 61:88-101.
[7]Vladimir Stevanovic, Milovan Studovic. 1994. A simple model for vertical annular and horizontal stratified two-phase flows with liquid entrainment and phase transitions one-dimensional steady state conditions.
[8]Sreenivas Jayanti, Michel Valette. 2003. Prediction of dryout and post-dryout heat transfer at high pressures using a one-dimensional three-fluid model.
[9]Satoru Sugawara, Yoshihiro Miyamoto. 1990. FIDAS: Detailed subchannel analysis code based on the three-fluid and three-field model. Nuclear Engineering and Design 120:147-161.
[10]Wallis GB. One-Dimensional Two-Phase Flow [M]. New York: McGraw-Hill, 1969.
[11]Clift R, Grace JR, Weber ME. Bubbles drops and particles [M]. New York: Academic press, 1978.
[12]Okawa T, Kotani A, Kataoka I, et al. 2004. Prediction of the critical heat flux in annular regime in various vertical channels. Nuclear Engineering and Design 229 (2–3): 223-236.
[13]Katto Y, Ohno H. 1984. An improved version of the generalized correlation of critical heat flux for the forced convective boiling in uniformly heated vertical tubes. International Journal of Heat and Mass Transfer 27 (9): 1641-1648.
[14]T. Ueda, M. Inoue, S. Nagatome. 1981. Critical heat flux and droplet entrainment rate in boiling of falling liquid films. International Journal of Heat and Mass Transfer 24 (7): 1257-1266.